RSC Advances

PAPER

View Article Online
View Journal | View Issue

Cite this: *RSC Adv.*, 2015, **5**, 6528

One pot synthesis of mesoporous boron nitride using polystyrene-*b*-poly(ethylene oxide) block copolymer†

Mahdi Maleki,*[ab] Ali Beitollahi,*[a] Jinwoo Lee,[b] Mohammadreza Shokouhimehr,[c] Jafar Javadpour,[a] Eun Ju Park,[d] Jinyoung Chun[b] and Jongkook Hwang[b]

Received 29th September 2014
Accepted 15th December 2014

DOI: 10.1039/c4ra11431k

www.rsc.org/advances

We report a successful synthesis of Mesoporous BN (MBN) powder through a facile one-pot synthesis strategy. In this respect, laboratory made block copolymer, polystyrene-*b*-poly(ethylene oxide) (PS-*b*-PEO) was used as structure directing agent and ammonia borane was used as BN precursor, respectively. Various characterization techniques such as X-ray photoelectron spectroscopy, Fourier-transform infrared spectroscopy, X-ray diffraction (XRD), scanning electron microscopy, transmission electron microscopy (TEM) and N_2 sorption analysis were used to characterize different properties of the synthesized MBN powder. The formation of turbostratic boron nitride with wormlike pores (20 nm) was confirmed by XRD and TEM results. N_2 sorption analysis of the obtained MBN sample exhibited a high specific surface area of 326 m^2 g^{-1} and a pore volume of 0.5 m^3 g^{-1}.

1. Introduction

Boron Nitride (BN) is one of the robust materials which displays interesting physical and chemical properties such as low density, excellent resistance to chemical attack, high melting point, good thermal conductivity, high oxidation resistance and biocompatibility.[1–7]

Porous BN due to its wide range of applications such as organic pollutant adsorption, water purification, energy storage, catalyst supports and field emission devices have recently received remarkable attention.[8–15] However, for most of these applications, the precise control of pore size/distributions, wall thickness, pore shape, specific surface area and surface chemistry is demanded. To achieve such goals, two major strategies known as hard and soft templates are normally utilized.

Mesoporous BN (MBN) has also been prepared by both of these synthetic routes as well. It is worth to mention that most of the previous studies have used mesoporous carbon or silica as the hard templates for the synthesis of MBN[16–19] and less attention has been paid to the soft template route using amphiphilic block copolymers (BCPs). The hard template method utilized for the synthesis of the MBN generally provides appropriate pore size and shape control through the pores of rigid template.[19] However, template removal, frequent replication and air sensitive precursors such as tri(methylamino)borazine (MAB) lend themselves as inevitable obstacles for facile synthesis of this material.[20,21]

Wan *et al.* reported a successful synthesis of highly ordered MBN by synthesizing a complex BCP, polynorbornene-*b*-polynorbornene decaborane (PNB-*b*-PDB).[22] Despite of the interesting results obtained by this group, however, the synthesis of such a complicated block copolymer is not an easy task.

Evaporation induced self assembly (EISA) method is appropriate procedure in the synthesis of mesoporous materials. In this respect, lab made BCPs such as PS-*b*-PEO (PSE) and poly(isoprene-*block*-ethyleneoxide) have been used for the synthesis of various mesoporous oxides such as TiO_2, Nb_2O_5, SiO_2 and carbon.[23–25] The composition, block sequence, molecular weight and volume fraction of the lab made BCPs can be tailored to earn suitable mesostructures.[26] However, for a successful synthesis of mesoporous materials using PSE, appropriate precursors and solvents should be attentively selected for either hydrophobic (PS) or hydrophilic (PEO) blocks.

In the synthesis of mesoporous SiO_2 through EISA method using PSE, the tetraethyl orthosilicate (TEOS) precursor can interact with the PEO segment of the BCPs.[27] The self assembly of (PEO-*b*-PS)/TEOS is occurred during solvent evaporation. In the case of mesoporous carbon, resol has a similar role with

[a]*Center of Excellence for Ceramic Materials in Energy and Environment Applications, School of Metallurgy & Materials Engineering, Iran University of Science and Technology (IUST), Narmak, Tehran 16846, Iran. E-mail: malekim@metaleng.iust.ac.ir; beitolla@iust.ac.ir; Fax: +98 21 77240480; Tel: +98 21 77459151*

[b]*Pohang University of Science and Technology (POSTECH), Chemical Engineering, Pohang, Republic of Korea*

[c]*School of Chemical and Biological Engineering, Seoul National University, Seoul 151-742, Republic of Korea*

[d]*Polymer Design & Reaction Engineering, Institute of Chemical and Engineering Sciences, Agency for Science, Technology and Research (A*STAR), 1 Pesek Road, Jurong Island, 627833, Singapore*

† Electronic supplementary information (ESI) available. See DOI: 10.1039/c4ra11431k

TEOS to interact with PEO block with hydrogen bonding to make a self assembled structure.[28] Heat treatment of self assembled BCP with resol/TEOS led to decomposition of BCP and formation of mesopores.[27,28]

Various BN precursors have been utilized by many research groups for the synthesis of porous BN powders such as MAB,[29] tri(chloro)borazine,[21] boron oxide[30–32] and boron tribromide (BBr_3).[33] Among these precursors, MAB has been frequently used due to appropriate micro-meso pores filling of carbon template and *in situ* thermal polymerization.[21] However, this compound is highly air–moisture sensitive making its handling difficult besides the fact that MAB is not commercially available. In contrast, ammonia borane (AB) or borazane as BN precursor is a nontoxic, non-explosive and stable crystalline compound under normal pressures and temperatures. It can be handled easily and it does not need any special facility compared to borazine compounds and can be solved in many polar solvents.[34–39] Furthermore, polymerization ability of AB as a necessary character for the precursors used in soft template route[39,40] and its commercially availability makes this compound as an appropriate candidate for the synthesis of MBN.

In this work, we report a novel procedure for the synthesis of MBN through self assembly of PSE as a structure directing agent and AB as BN precursor through a simple one-pot EISA method.

2. Experimental

2.1. Chemicals

Monomethoxy PEO5000 (mPEO5000), 2-bromoisobutyryl bromide ($(CH_3)_2CBrCOBr$), pentamethyldiethylenetriamine (PMDETA), tetrahydrofuran (THF), triethylamine (TEA), styrene ($C_6H_5CH{=}CH_2$), methanol (CH_3OH), copper bromide (CuBr), ethanol (EtOH) and ammonia borane (97%) were purchased from Sigma-Aldrich. mPEO5000 dissolved in 100 ml of toluene was distilled to remove the water in the PEO chain. Styrene was filtered using neural Al_2O_3 column to eliminate the inhibitor.

2.2. Preparation of PS-*b*-PEO diblock copolymer

Laboratory made BCP, PS-*b*-PEO, with Mn = 26 000 g mol^{-1}, polydispersity index PDI = 1.2 and 23.7 wt% of PEO was prepared *via* an atom transfer radical polymerization (ATRP) method.[41] First, PEO–Br macroinitiator was prepared by adding 2-bromoisobutylbromide (1.48 ml) into PEO–OH (20 g) dissolved in the solution of CH_2Cl_2 (200 ml) and triethylamine (5 ml). After 8 h of stirring at room temperature, PEO–Br was precipitated in cold ether and dried at room temperature. Secondly, chain extension from PEO–Br to PEO-*b*-PS was conducted. PEO–Br (2.539 g, 0.5 mmol), styrene (20 g, 192 mmol), CuBr (0.071 g, 0.5 mmol) and PMDETA (0.085 g, 0.5 mmol) were placed in 50 ml round bottom flask. N_2 bubbling and freeze–pump–thaw were conducted to remove oxygen and water. After 5 h of polymerization at 110 °C, resulting viscous solution was diluted in THF and filtered using alumina column to remove copper catalyst. The filtered solution was precipitated in cold methanol and the resulting white power was dried under vacuum at room temperature.[41]

2.3. Synthesis of MBN

In a typical synthesis, 0.1 g PSE was dissolved in THF : EtOH with 3 : 2 volume ratios at room temperature under stirring condition. After complete dissolving of PSE, 0.1 g AB was added to BCP solution under mixing condition. The prepared solution was stirred for 2 h at room temperature and then cast on a petri-dish placed on a hot plate at 50 °C. Films were aged at 50 °C (24 h), 80 °C (6 h) and 100 °C for 24 h. The as-made film was crushed and heat treated using heating program 1 °C min^{-1} ramp to 200 °C (for 2 h) and 1.4 °C min^{-1} ramp to 1150 °C (for 2 h) under ammonia atmosphere. Heat treatment regime was selected based on the thermal analysis carried out under argon atmosphere (as presented in the ESI, Fig. S1†). In order to study the effect of AB in the micropores formation, polymerized AB at 80 °C was also subjected to a similar heat treatment regime used for AB/PSE samples.

2.4. Characterization

Structural analysis was carried out using an X-ray diffraction (XRD) technique by a MAX-2500 diffractometer (RIKAGU, CuK_α, 1.54 Å). Fourier-transformed infrared (FTIR) spectra were recorded on a Perkin Elmer spectrophotometer between 500 and 4000 cm^{-1}, using KBr pellets. Thermogravimetric analysis (TGA) and differential scanning calorimetry (DSC) method were performed under nitrogen and air atmospheres at different heating rates 3, 10 °C min^{-1}.

^{11}B NMR spectra were recorded on Solid/Micro-Imaging High Resolution NMR AVANCE 400 WB operating at 128.28 MHz. Chemical shifts were referenced to $BF_3(OEt)_2$ ($\delta = 0$ ppm). X-ray photoelectron spectroscopy (XPS) measurements were carried out for the prepared MBN using AXIS Ultra DLD, Kratos Inc, employing Mg K_α lines (1486.6 eV) as an excitation source. The carbonaceous C 1s line (284.6 eV) was used as the reference to calibrate the binding energies.

Nitrogen physisorption was measured using Micromeritics Tristar II system at −196 °C. The samples were degassed at 150 °C before measurements. The Brunauer–Emmett–Teller (BET) method was utilized to calculate the specific surface area (S_{BET}) using the adsorption branch. The pore size distribution (PSD) was derived from the adsorption branch by using the Barrett–Joyner–Halenda (BJH) model. The total pore volume (V_{total}) was estimated from the adsorbed amount at $P/P_0 = 0.995$. In order to determine micropore volume, the Dubinin–Raduskevitch (DR) theory was used.[18]

The microstructural analyses were carried out using a scanning electron microscopy (SEM) JEOL JSM-6330F and a transmission electron microscopy (TEM) Philips Tecnai 20. The prepared powders were dispersed in EtOH and deposited on to carbon coated grid and left to dry at room temperature before the TEM analysis.

3. Results and discussion

3.1. Interaction of AB and PSE

Fig. 1 shows the XRD spectra of the AB and AB/PSE samples after evaporation of the solvents at 50 °C. The XRD spectrum of

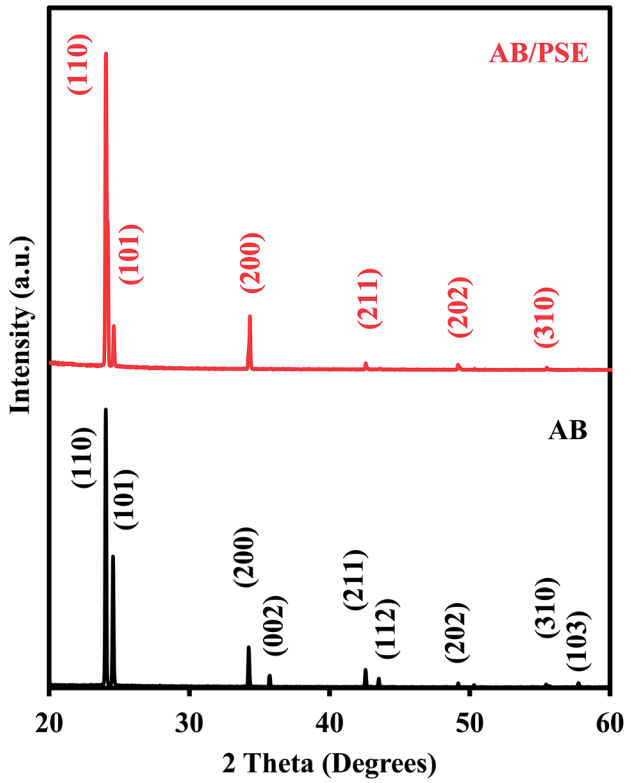

Fig. 1 XRD spectra of AB and AB/PSE after evaporation of solvent at 50 °C.

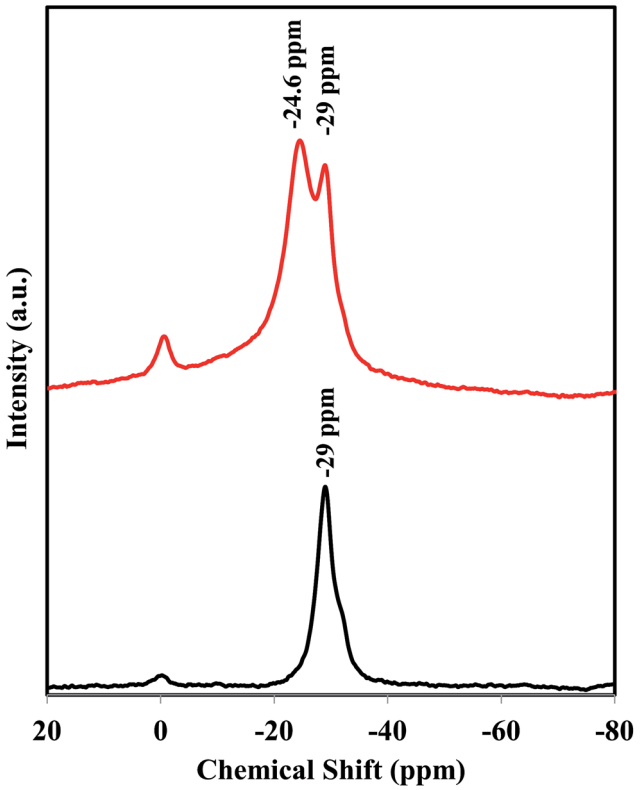

Fig. 2 Solid state ^{11}B NMR spectra of AB and AB/PSE after evaporation of solvent at 50 °C.

AB in Fig. 1 reveals peaks at 24, 24.5, 34.2, 35.7, 42.6, 43.5, 49.2, 55.4 and 57.7 degrees. The observed peaks are respectively assigned to (110), (101), (200), (002), (211), (112), (202), (310) and (103) reflections in tetragonal structure of AB (JCPDS Card no. 13-0292). The XRD peaks of AB/PSE compared to AB reveals that the intensity ratio of crystallographic planes of (101) and (110) has been changed. Further, peaks of (002), (112) and (103) were disappeared after hybrid formation. In other word, PSE confined the growth of AB in this direction. This possibly happened by crystallographic orientation of AB.

In order to understand the possible set up of interaction between AB and PSE, the samples were characterized by solid state ^{11}B NMR. The ^{11}B NMR spectra of AB and AB/PSE are shown in Fig. 2. Compared to AB ^{11}B NMR peak (−29 ppm), ^{11}B NMR spectrum of AB/PSE hybrid has an extra peak at −24.6 ppm.

W. J. Shaw *et al.*[42] has also reported the appearance of rather similar extra peak for AB subjected to thermal decomposition at 80 °C. This was attributed to the formation of highly mobile (BH_3NH_3) molecules. Furthermore, they have also noticed the existence of such peak for AB scaffolded in MCM-41.[42] This was related to highly mobile molecule due to breaks up the 3-dimensional dihydrogen bonding network.[42] Further, similar phase was also observed due to interaction between AB and polyetheral promoters.[43] The observed peak at −24.6 ppm (Fig. 2) for AB/PSE samples studied could be possibly due to the formation of such new mobile molecules.

FTIR spectroscopy was used to further investigate the interactions between AB and PSE. Fig. 3a–d shows the FTIR spectra of the AB, PSE and AB/PSE samples (with two different weight ratios: 1 : 1 and 1 : 15) after evaporation of the solvent for the latter at 50 °C.

Fig. 3a shows peaks at 3318, 2344, 1610, 1379, 1163, 1065, 782, 729 cm^{-1} for AB. The observed peak at 3318 cm^{-1} is assigned to NH stretching modes and peak near 2344 cm^{-1} is assigned to BH stretching mode.[44] The detected peaks at 1610 cm^{-1} and 1379 cm^{-1} are due to NH_3 deformations, and peak at 1165 cm^{-1} is assigned to BH_3 deformations.[44] The peaks at 1065 cm^{-1} and 729 cm^{-1} have been attributed to NBH rocking modes. The peak at 782 cm^{-1} is due to B–N bond in AB.[44] The appeared peaks in Fig. 3b at 3026, 1601, 1493, 1452, 843 and 698 cm^{-1} are related to polystyrene and the emerged peaks at 1148 and 1108 cm^{-1} are assigned to PEO block in PSE BCP made by ATRP method.[28,45,46]

FTIR peaks comparison of the AB, PSE and AB/PSE samples showed that PS peaks have minimum chemical shift after AB/PSE hybrid formation as it was also confirmed by Kurban finding about interaction between AB and PS.[47] The presence of a peak in a similar position for B–N bond (781 cm^{-1}) in AB and AB/PSE (782 cm^{-1}) confirms the existence of such bond in AB/PSE as well. B–H peaks of AB/PSE compared to AB have shifted to higher wave numbers from 1064 cm^{-1} to 1057 cm^{-1} and 2344 cm^{-1} to 2352 cm^{-1} (Fig. 2c). As it can be noticed from Fig. 2d, the N–H peak of AB has shifted from 3317 cm^{-1} to lower

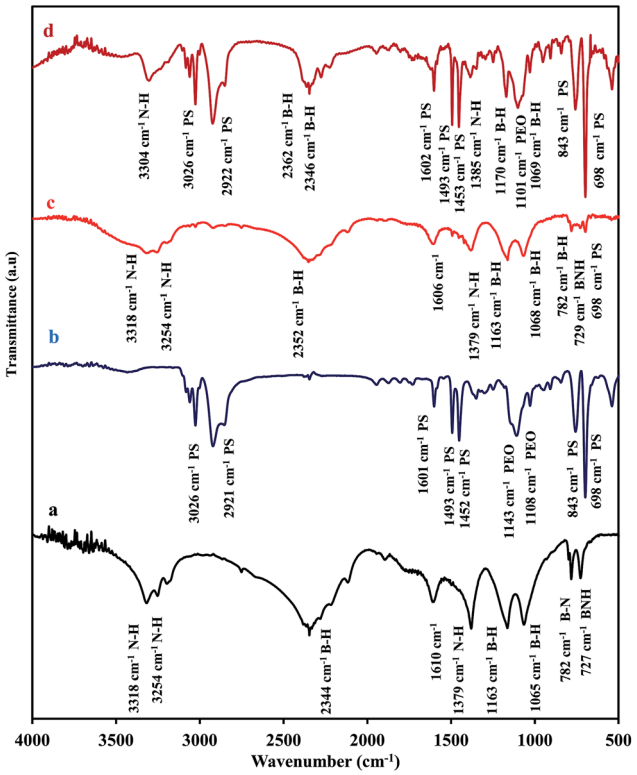

Fig. 3 FTIR spectra of (a) AB, (b) PSE, (c) AB/PSE: 1/1 and (d) AB/PSE: 1/15 (weight ratio) after evaporation of solvent at 50 °C.

wave number (3304 cm^{-1}) due to the weakening of the N–H stretching bond. On the other hand, the observed increase of N–H_3 bending mode bond peak position from 1379 cm^{-1} to 1385 cm^{-1} can be possibly due to change of AB configuration and N–H_3 bending bonds.

Previous studies[43,48] have also considered interaction between AB with other polymers. For instance, the results of Zhao group[48] demonstrated that AB binds to methyl methacrylate polymer through hydrogen bonding between hydrogen in B–H bond and oxygen of polymer. Further, Kim *et al.* declared that hydrogen of the N–H bond is the agent of hydrogen bonding between AB and oxygen atom of ethereal polymer.[43]

For the investigated samples in this work, in addition to XRD and ^{11}B NMR studies, the N–H stretching bond weakening and B–H strengthening bonds suggest that AB could be possibly connected to oxygen atom of PEO through the N–H bond of AB.[48] However, this demanded further study by more details analysis.

As it was mentioned before, key controlling factor in the synthesis of mesoporous materials such as TiO_2, SiO_2 and carbon through EISA methods using BCPs is the compatibility between hydrophilic blocks of BCPs and inorganic precursors. W. Luo reported that hydroxyl groups of resol can form hydrogen-bonding with EO-containing block polymers and are arranged around block copolymer micelles.[49] In the synthesis of MBN with PNB-*b*-PDB, also tried to connect the BN precursor (decaborane) to polynorbornene block before BCP preparation.[22] Pyrolysis of self assembled PNB-*b*-PDB under ammonia atmosphere led to decomposition of the PNB and formation of mesopores.

As AB does not have interaction with PS, AB selectively incorporates in hydrophilic PEO block of BCP and swells hydrophilic part to form corona while the PS forms rigid core. Casting the solution in the petri-dish leads to evaporation of solvent (Scheme 1). Evaporation induced self assembly of PSE/AB precursors leads to form a white film. Pyrolysis at high temperature (1150 °C) for the as-made film under ammonia atmosphere further involves the substitution of carbon with

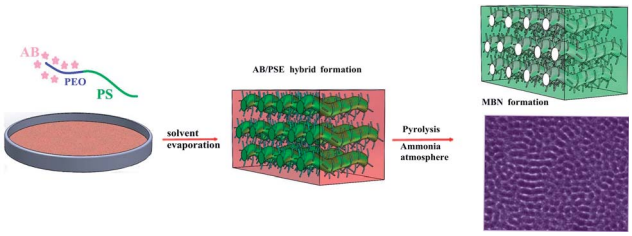

Scheme 1 Diagram of synthesis of the MBN powder through self-assembly of AB and PSE.

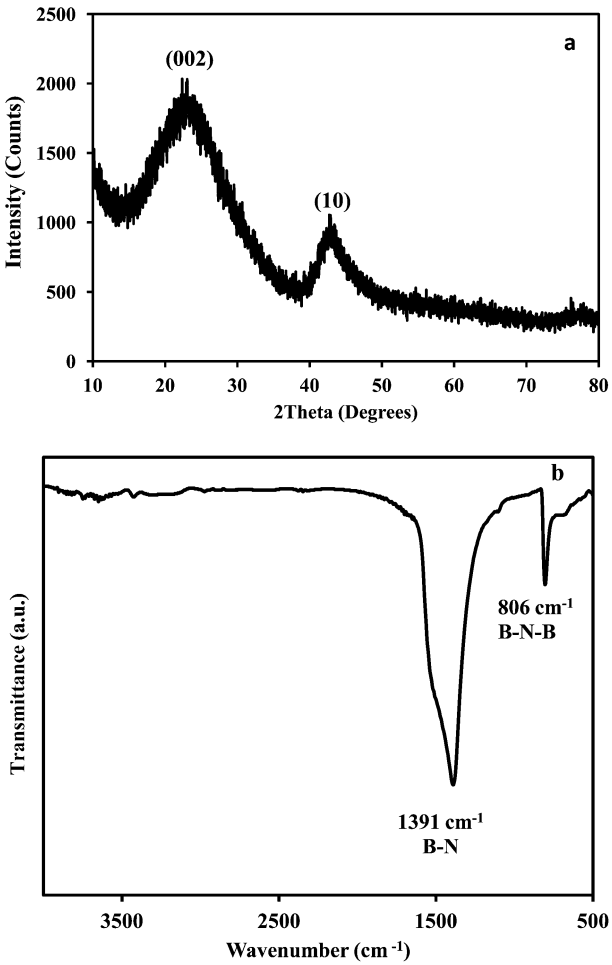

Fig. 4 a) X-ray diffraction pattern and (b) FTIR spectrum of the MBN prepared by one-pot method.

nitrogen, eventually leading to the formation of MBN with white color.[22]

3.2. Structural and chemical analysis of MBN

Fig. 4a reveals XRD pattern of the prepared MBN powder after heat treatment under ammonia atmosphere at 1150 °C. The appearance of the two broad peaks at 24–26° and 43–46° are attributed to (002) and unresolved (10) reflections of turbostratic BN phase with low crystalline BN structure.[50] The broadened peaks indicate the possible presence of highly defective and randomly stacked layers of the BN sample.

Fig. 4b exhibits a typical FTIR spectrum of the prepared MBN powder with two main characteristic absorption peaks around 1384 cm^{-1} and 798 cm^{-1}. The former peak can be attributed to the stretching vibration of the B–N bond, while the latter one is corresponding to the out-of-plane bending vibrations of B–N–B bond.[19] The weak bands around 3430 cm^{-1} and 3250 cm^{-1} can be also assigned to ν(N–H) and ν(BOH) vibrations.[50]

The XPS survey scan spectrum and deconvoluted XPS spectra of B 1s and N 1s from MBN powder are depicted in Fig. 5. Deconvolution of B 1s spectrum gives two peaks centered at 190.27 eV and 192.38 eV. The dominant peak of the B 1s spectrum is located at 190.27 eV (Fig. 5), which is attributable to B 1s of B–N bonds. The small peak at high energy (192.38 eV) is assigned to B–O bonds and can be due to air exposure of the sample or surface contamination.[31,51–53] The observed peak at 39 8.09 eV is attributed to N 1s spectrum (398.1 eV) of B–N bond.[54] Both B 1s and N 1s spectra indicate that the main configuration of B and N atoms are related to the B–N bonds. The atomic percentage of B, N, C and O from XPS spectra were 42.1%, 37.3%, 7.9% and 12.7%, respectively. The B/N atomic ratio from our XPS survey was about 1.1 which is near to the BN stoichiometry.

3.3. Thermal analysis of MBN

In order to investigate the weight change of the as-prepared MBN, the TGA analysis was carried out up to 800 °C in the air atmosphere (Fig. 6). TGA result indicated that the product has near 10% weight loss below 200 °C. This is related to adsorbed H_2O or CO_2. As it can be observed from TGA graph, no weight gain that is sign of BN oxidation to B_2O_3 was noticed in the applied temperature range. Based on TGA, we suggest that the MBN samples are stable. However, further investigations are required, in particular by BET analysis on the air-treated sample, to confirm the stability of the obtained powders.

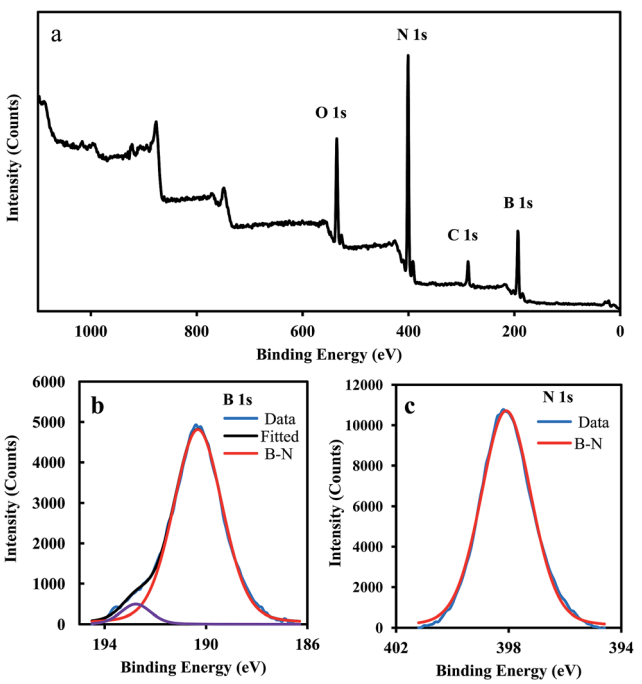

Fig. 5 B 1s, N 1s and survey scan XPS spectra of the MBN prepared by one pot method.

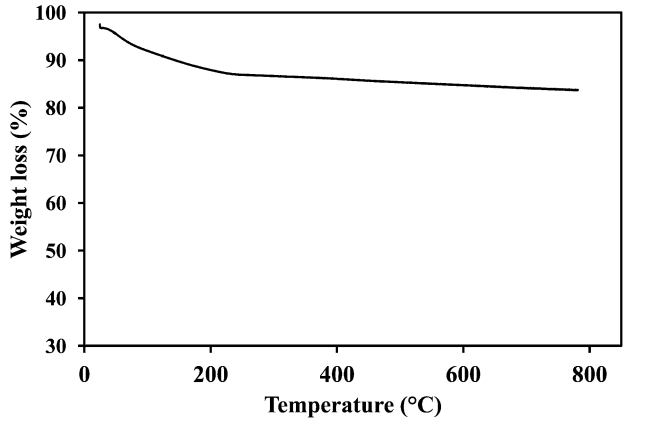

Fig. 6 TGA analysis of MBN under air atmosphere at a heating rate of 10 °C min^{-1}.

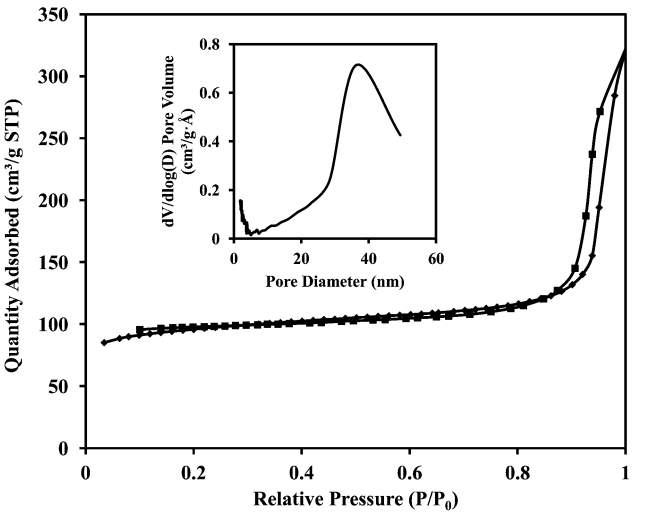

Fig. 7 Nitrogen adsorption–desorption isotherm and PSD (BJH) of the MBN prepared by PSE block copolymer.

3.4. Surface area study of MBN

The nitrogen sorption isotherm of the prepared MBN corresponds to type-IV curve with a sharp adsorption at ~0.9 P/P_0, indicating the presence of large dominant pores (Fig. 7). PSD analysis determined from the adsorption isotherm branch shows the pores with 36 nm in diameter. The obtained BET surface area and pore volume and micropore volume (DR theory) were 326 $m^2\ g^{-1}$, 0.5 $m^3\ g^{-1}$ and 0.1 $cm^3\ g^{-1}$, respectively.

3.5. MBN microstructure analysis

Fig. 8a shows a SEM micrograph of MBN produced by the designed one-pot method. It can be seen that wormlike mesopores with 20 nm in diameter were formed. Furthermore, TEM results also confirmed the formation of worm like mesoporous boron nitride as well (Fig. 8b). The inset of Fig. 8b demonstrates the image of formed micropores in the synthesized product.

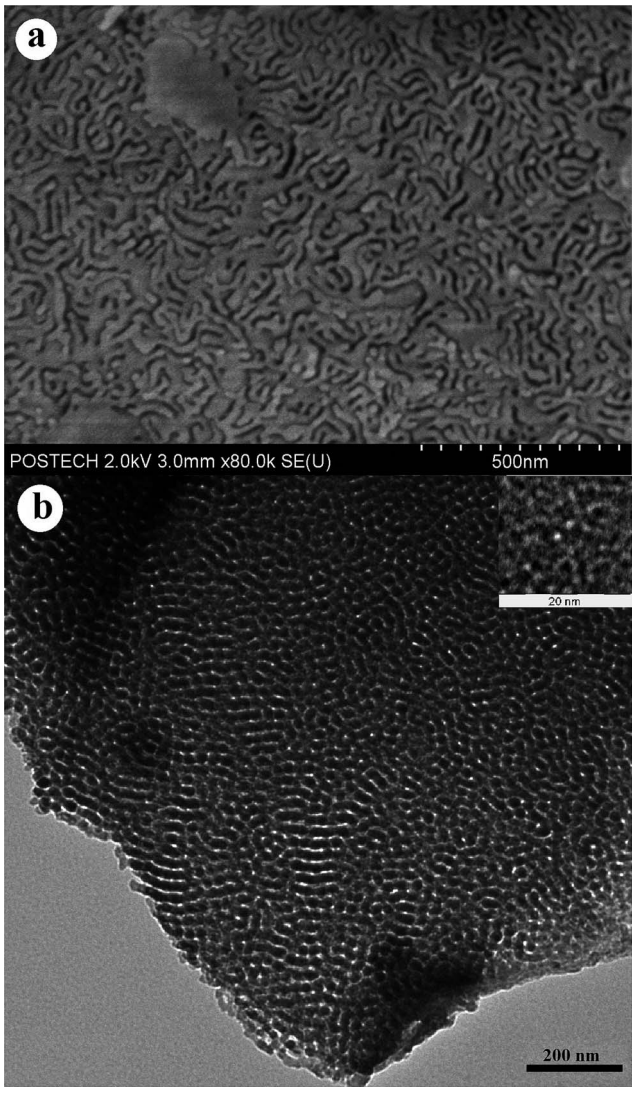

Fig. 8 (a) SEM and (b) TEM images of the MBN prepared by one pot method. The inset shows a TEM image of micropores in the prepared MBN.

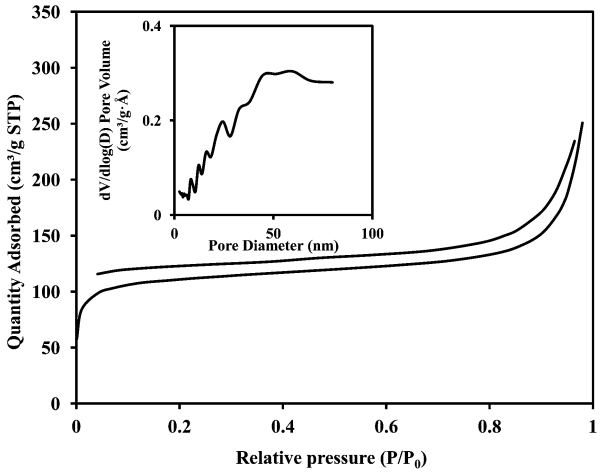

Fig. 9 Nitrogen adsorption–desorption isotherm and BJH pore size distribution of polymerized AB after heat treatment at 1150 °C under ammonia atmosphere.

3.6. Micropores sources

As it can been seen in Fig. 5, the isotherm branch has a long horizontal part that is characteristic of microporous materials.[55] In addition to isotherm branch, the TEM picture in Fig. 8b demonstrated formation of micropores. The formation of micropores in the mesoporous materials could be due to several parameters. Mutually interpenetrating network of silica and hydrophilic EO chains formed during the assembly of the organic/inorganic hybrid material led to microporosity.[56] Also PEO decomposition in mesoporous silica which has been prepared with PS-*b*-PEO block copolymer led to micropores formation.[23]

For the prepared MBN powder in this work, the thermal decomposition of interpenetrating of PEO in AB network is considered as one of the micropores resources.

Furthermore, precursor polymerization could be one of the micropores sources.[57] It was indicated that the polymerization of polymeric BN precursors leads to microporosity in BN ceramic.[58–60] In order to investigate the contribution of AB thermal decomposition in the micropores formation, AB was polymerized at 80 °C for 16 h. Then the polymerized AB was heat treated using a similar heating program used for AB/PSE hybrid under ammonia atmosphere at 1150 °C for 2 h. Fig. 9 shows the nitrogen sorption isotherm of polymerized AB after heat treatment under ammonia atmosphere. Surprisingly, the surface area was 480 $m^2\ g^{-1}$ and micropore volume was 0.177 $cm^3\ g^{-1}$. Moreover, as it can be seen from Fig. 9, beginning of absorption isotherm from low relative pressure demonstrates presence of micropores.[61] Therefore, the set up of micropores for the MBN powders synthesized here could be possibly originated from AB and PEO thermal decomposition.

4. Conclusions

In summary, wormlike mesoporous BN has been successfully prepared by a simple one-pot synthesis procedure through heat

treatment of self assembled PSE with AB under ammonia atmosphere at 1150 °C. Surface area, pore volume and micropore volume of the wormlike mesoporous BN prepared by this method were 326 $m^2\ g^{-1}$, 0.5 $m^3\ g^{-1}$ and 0.1 $cm^3\ g^{-1}$, respectively. Thermal heat treatment of AB separately exhibited that the part of microporosity was originated by AB.

Notes and references

1 V. Salles, S. Bernard, A. Brioude, D. Cornu and P. Miele, *Nanoscale*, 2010, **2**, 215–217.
2 R. T. Paine and C. K. Narula, *Chem. Rev.*, 1990, **90**, 73.
3 Z. Liu, Y. Gong, W. Zhou, L. Ma, J. Yu, J. C. Idrobo, J. Jung, A. H. MacDonald, R. Vajtai, J. Lou and P. M. Ajayan, *Nat. Commun.*, 2013, **4**, 1.
4 J. A. Perdigon-Melon, A. Auroux, D. Cornu, P. Miele, B. Toury and B. Bonnetot, *J. Organomet. Chem.*, 2002, **657**, 98.
5 C. Zhi, N. Hanagata, Y. Bando and D. Golberg, *Chem.–Asian J.*, 2011, **6**, 2530.
6 C. Zhi, Y. Xu, Y. Bando and D. Golberg, *ACS Nano*, 2011, **5**, 6571.
7 G. Ciofani, V. Raffa, A. Menciassi and A. Cuschieri, *Biotechnol. Bioeng.*, 2008, **101**, 850.
8 Q. Weng, X. Wang, C. Zhi, Y. Bando and D. Golberg, *ACS Nano*, 2013, **7**, 1558.
9 M. Terrones, J. C. Charlier, A. Gloter, E. Cruz-Silva, E. Terrés, Y. B. Li, A. Vinu, Z. Zanolli, J. M. Dominguez, H. Terrones, Y. Bando and D. Golberg, *Nano Lett.*, 2008, **8**, 102.
10 X. L. Meng, N. Lun, Y. X. Qi, H.-L. Zhu, F. D. Han, L. W. Yin, R. H. Fan, Y. J. Bai and J. Q. Bi, *J. Solid State Chem.*, 2011, **184**, 859.
11 C. J. H. Jacobsen, *J. Catal.*, 2001, **200**, 1.
12 J. A. Perdigon-Melon, A. Auroux, C. Guimon and B. Bonnetot, *J. Solid State Chem.*, 2004, **177**, 609.
13 M. Wang, M. Li, L. Xu, L. Wang, Z. Ju, G. Li and Y. Qian, *Catal. Sci. Technol.*, 2011, **1**, 1159.
14 X. Zhang, G. Lian, S. Zhang, D. Cui and Q. Wang, *CrystEngComm*, 2012, **14**, 4670.
15 J. Kim, J. Han, M. Seo, S. Kang, D. Kim and J. Ihm, *J. Mater. Chem. A*, 2013, **1**, 1014.
16 P. Dibandjo, F. Chassagneux, L. Bois, C. Sigala and P. Miele, *J. Mater. Chem.*, 2005, **15**, 1917.
17 P. Dibandjo, L. Bois, C. Estournes, B. Durand and P. Miele, *Microporous Mesoporous Mater.*, 2008, **111**, 643.
18 S. Schlienger, J. Alauzun, F. Michaux, L. Vidal, J. Parmentier, C. Gervais, F. Babonneau, S. Bernard, P. Miele and J. B. Parra, *Chem. Mater.*, 2011, **24**, 88.
19 P. Dibandjo, F. Chassagneux, L. Bois, C. Sigala and P. Miele, *Microporous Mesoporous Mater.*, 2006, **92**, 286.
20 P. Dibandjo, L. Bois, F. Chassagneux, D. Cornu, J.-M. Letoffe, B. Toury, F. Babonneau and P. Miele, *Adv. Mater.*, 2005, **7**, 571.
21 P. Dibandjo, F. Chassagneux, L. Bois, C. Sigala and P. Miele, *J. Mater. Res.*, 2007, **22**, 26.
22 R. L. MalenfantPatrick, J. Wan, S. T. Taylor and M. Manoharan, *Nat. Nanotechnol.*, 2007, **2**, 43.
23 B. Smarsly, G. Xomeritakis, K. Yu, N. Liu, H. Fan, R. A. Assink, C. A. Drewien, W. Ruland and C. J. Brinker, *Langmuir*, 2003, **19**, 7295.
24 J. Lee, M. Christopher Orilall, S. C. Warren, M. Kamperman, F. J. DiSalvo and U. Wiesner, *Nat. Mater.*, 2008, **7**, 222.
25 Y. J. Cheng and J. S. Gutmann, *J. Am. Chem. Soc.*, 2006, **128**, 4658.
26 Y. Deng, J. Wei, Z. Sun and D. Zhao, *Chem. Soc. Rev.*, 2013, **42**, 4054.
27 Y. Y. Li, J. Wei, W. Luo, C. Wang, W. Li, S. Feng, Q. Yue, M. Wang, A. A. Elzatahry, Y. Deng and D. Zhao, *Chem. Mater.*, 2014, **26**, 2438.
28 Y. Deng, T. Yu, Y. Wan, Y. Shi, Y. Meng, D. Gu, L. Zhang, Y. Huang, C. Liu, X. Wu and D. Zhao, *J. Am. Chem. Soc.*, 2007, **129**, 1690.
29 P. Dibandjo, L. Bois, F. Chassagneux, J. M. Letoffe and P. Miele, *J. Porous Mater.*, 2008, **15**, 13.
30 W. Q. Han, R. Brutchey, T. D. Tilley and A. Zettl, *Nano Lett.*, 2003, **4**, 173.
31 W. Lei, D. Portehault, D. Liu, S. Qin and Y. Chen, *Nat. Commun.*, 2013, **4**, 1777.
32 J. Li, J. Lin, X. Xu, X. Zhang, Y. Xue, J. Mi, Z. Mo, Y. Fan, L. Hu, X. Yang, J. Zhang, F. Meng, S. Yuan and C. Tang, *Nanotechnology*, 2013, **24**, 155603.
33 M. Zheng, Y. Liu, Y. Gu and Z. Xu, *Sci. China, Ser. B: Chem.*, 2008, **51**, 205.
34 M. P. Mitoraj, *J. Phys. Chem. A*, 2011, **115**, 14708.
35 X. Wang, A. Pakdel, C. Zhi, K. Watanabe, T. Sekiguchi, D. Golberg and Y. Bando, *J. Phys.: Condens. Matter*, 2012, **24**, 314205.
36 P. V. Ramachandran and P. D. Gagare, *Inorg. Chem.*, 2007, **46**, 7810.
37 Y. Zhao, J. Zhang, D. L. Akins and J. W. Lee, *Ind. Eng. Chem. Res.*, 2011, **50**, 10024.
38 J. S. Wang and R. A. Geanangel, *Inorg. Chim. Acta*, 1988, **148**, 185.
39 S. Frueh, R. Kellett, C. Mallery, T. Molter, W. S. Willis, C. King'ondu and S. L. Suib, *Inorg. Chem.*, 2010, **50**, 783.
40 C. J. Brinker, Y. Lu, A. Sellinger and H. Fan, *Adv. Mater.*, 1999, **11**, 579.
41 J. Hwang, J. Kim, E. Ramasamy, W. Choi and J. Lee, *Microporous Mesoporous Mater.*, 2011, **143**, 149.
42 W. J. Shaw, M. Bowden, A. Karkamkar, C. J. Howard, D. J. Heldebrant, N. J. Hess, J. C. Linehan and T. Autrey, *Energy Environ. Sci.*, 2010, **3**, 796.
43 Y. Kim, H. Baek, J. H. Lee, S. Yeo, K. Kim, S.-J. Hwang, B. Eun, S. W. Nam, T. H. Lim and C. W. Yoon, *Phys. Chem. Chem. Phys.*, 2013, **15**, 19584.
44 N. J. Hess, M. E. Bowden, V. M. Parvanov, C. Mundy, S. M. Kathmann, G. K. Schenter and T. Autrey, *J. Chem. Phys.*, 2008, **128**, 34508.
45 M. Zhang, L. Yang, S. Yurt, M. J. Misner, J. T. Chen, E. B. Coughlin, D. Venkataraman and T. P. Russell, *Adv. Mater.*, 2007, **19**, 1571.
46 G. Wang and J. Huang, *J. Polym. Sci., Part A: Polym. Chem.*, 2008, **46**, 1136.

47 Z. Kurban, A. Lovell, S. M. Bennington, D. W. K. Jenkins, K. R. Ryan, M. O. Jones, N. T. Skipper and W. I. F. David, *J. Phys. Chem. C*, 2010, **114**, 21201.
48 J. Zhao, J. Shi, X. Zhang, F. Cheng, J. Liang, Z. Tao and J. Chen, *Adv. Mater.*, 2010, **22**, 394.
49 W. Luo, Y. Li, J. Dong, J. Wei, J. Xu, Y. Deng and D. Zhao, *Angew. Chem., Int. Ed.*, 2013, **52**, 10505.
50 P. Dibandjo, L. Bois, F. Chassagneux and P. Miele, *J. Eur. Ceram. Soc.*, 2007, **27**, 313.
51 C. Guimon, D. Gonbeau, G. Pfister-Guillouzo, O. Dugne, A. Guette, R. Naslain and M. Lahaye, *Surf. Interface Anal.*, 1990, **16**, 440.
52 Q. Weng, X. Wang, Y. Bando and D. Golberg, *Adv. Energy Mater.*, 2013, 1301525.
53 J. G. Alauzun, S. Ungureanu, N. Brun, S. Bernard, P. Miele, R. Backov and C. Sanchez, *J. Mater. Chem.*, 2011, **21**, 14025.
54 L. Ci, L. Song, C. Jin, D. Jariwala, D. Wu, Y. Li, A. Srivastava, Z. F. Wang, K. Storr, L. Balicas, F. Liu and P. M. Ajayan, *Nat. Mater.*, 2010, **9**, 430.
55 B. Xu, S. Hou, H. Duan, G. Cao, M. Chu and Y. Yang, *J. Power Sources*, 2013, **228**, 193.
56 C. M. Yang, B. Zibrowius, W. Schmidt and F. Schüth, *Chem. Mater.*, 2004, **16**, 2918.
57 L. Zhang, Q. Yang, H. Yang, J. Liu, H. Xin, B. Mezari, P. C. M. M. Magusin, H. C. L. Abbenhuis, R. A. v. Santen and C. Li, *J. Mater. Chem.*, 2008, **18**, 450.
58 J. F. Janik, W. C. Ackerman, R. T. Paine, D.-W. Hua, A. Maskara and D. M. Smith, *Langmuir*, 1994, **10**, 514.
59 T. T. Borek, W. Ackerman, D. W. Hua, R. T. Paine and D. M. Smith, *Langmuir*, 1991, **7**, 2844.
60 D. A. Lindquist, T. T. Borek, S. J. Kramer, C. K. Narula, G. Johnston, R. Schaeffer, D. M. Smith and R. T. Paine, *J. Am. Ceram. Soc.*, 1990, **73**, 757.
61 N. Brun, S. R. S. Prabaharan, C. Surcin, M. Morcrette, H. Deleuze, M. Birot, O. Babot, M.-F. Achard and R. Backov, *J. Phys. Chem. C*, 2011, **116**, 1408.